CONFERENCE PRE-PRINT

ITER DISRUPTION MITIGATION SYSTEM DESIGN AND APPLICATION STRATEGY

S. JACHMICH¹, M. LEHNEN¹†, U. KRUEZI¹, F.J. ARTOLA¹, M. DIBON¹, S. GIORS¹, M. KOCHERGIN¹, A. LOARTE¹, T. LUCE¹.², R.A. PITTS¹, L.R. BAYLOR³, T. BOUJET⁴, D. DUNAI⁵, T.E. GEBHART³, Á. GYENGE⁶, A. HORVAT⁷, G. KOCSISፆ, J. MANZAGOL⁴, A. MATSUYAMAፆ, P. MATURA¹⁰, F. MILLET⁴, E. NARDON¹¹, D.I. RÉFYፆ, U. SHEIKH¹², S. SIGNETTI¹⁰, T. SZEPESIፆ, I.V. VINYAR¹³, S. ZOLETNIKፆ, A. ZSÁKAIፆ

- ¹ ITER Organization, Route de Vinon, CS 90 046, 13067 Saint Paul Lez Durance, France
- ² Princeton Plasma Physics Laboratory, Princeton, New Jersey, U.S.
- ³ Oak-Ridge National Laboratory, Oak Ridge, U.S.
- ⁴ Univ. Grenoble Alpes, CEA, IRIG-DSBT, F-38000 Grenoble, France
- ⁵ Fusion Instruments Kft, Budapest, Hungary
- ⁶ Budapest Univ. of Technology and Economics, Fac. of Mech. Eng., Dept. of Fluid Mech., 1111 Budapest, Hungary
- ⁷ Caspus, Oxford, United Kingdom of Great Britain and Northern Ireland
- ⁸ HUN-REN Centre for Energy Research, Institute for Atomic Energy Research, 1121 Budapest, Hungary
- ⁹ Graduate School of Energy Science, Kyoto University, Uji, Japan
- ¹⁰ Fraunhofer Institute for High-Speed Dynamics, Ernst-Mach-Institut, EMI, 79104 Freiburg im Breisgau, Germany
- ¹¹CEA/IRFM, Saint-Paul-Lez-Durance, France
- ¹² Ecole Polytechnique Fédérale de Lausanne (EPFL), Swiss Plasma Center (SPC), CH-1015 Lausanne, Switzerland
- ¹³PELIN, LLC, 18A, Grazhdanskaya, Saint Petersburg 190031, Russia

Email: stefan.jachmich@iter.org

Abstract

ITER will be equipped with a sophisticated disruption mitigation system based on shattered pellet injection. An R&D program has been launched to overcome the challenges that the design and integration of the system in the ITER environment are posing. Novel concepts for the various processes involved for injecting cryogenic fragments of low-Z and high-Z material are presented. Already in early phases of the execution of the ITER Research Plan, the DMS must be reliable and optimised for the range of discharges that will need to be executed for the development of the Research Plan. The viability of different injection schemes to achieve the required mitigation is summarised.

1. INTRODUCTION

The ITER Disruption Mitigation System (DMS) is essential to protect the ITER components from excessive heat and electromagnetic loads. Its design has reached a high maturity and successfully passed its final design review in 2024. It is based on shattered pellet injection (SPI) technology to deliver massive quantities of protium (H) and neon (Ne) to the plasma. Its main functions may be summarized as follows:

- 1) dissipation of the thermal and magnetic energy by Ne line radiation;
- 2) control of the current decay time to minimise electromagnetic loads;
- 3) avoidance of runaway electron (RE) formation through fuelling with H to increase the plasma density and reduce the temperature;
- 4) mitigation of the RE energy impact either through collisional dissipation following Ne injection, or through the control of the RE energy deposition phase by injecting tailored amounts of H.

Although the efficacy of SPI for disruption mitigation has been demonstrated on various tokamaks [1-7], with pellet injection systems for various pellet sizes commonly available [8-11], a very significant effort has been dedicated to the establishment of the physics basis for the DMS design requirements [12]. Important parameters of the design specifications are presently being reviewed and consolidated. Similarly, a dedicated and intense R&D programme has been required to find and validate novel solutions for numerous technological challenges, arising from the first-of-kind nature of the ITER DMS (e.g. the harsh environment due to neutron bombardment and ambient magnetic field and the high availability and reliability demands). These joint physics and technology efforts were conducted within the auspices of the international DMS Task Force (DMS TF) established by the ITER Organization in 2018 [13].

1

[†] Deceased

2. ITER DMS DESIGN

The DMS consists of 27 shattered pellet injectors distributed over 3 equatorial ports (EP), see example in Fig. 1, and 3 upper port (UP) cells. Upon receipt of a trigger from the Advanced Protection System it can inject within ~17 ms up to ~42 mol of protium (H), 70 mol of neon (Ne) or mixtures thereof in the form of cryogenic fragments.

The number of injectors and locations allow injections to be adapted to different phases of the discharge with different plasma parameters while still providing sufficient redundancy to ensure high availability of the system. Initial design specifications had been defined to allow the design to progress. These include pellet size and velocity, fragment sizes their velocity dispersion, synchronisation needs for multiple injections, precision of the pellet composition, etc.

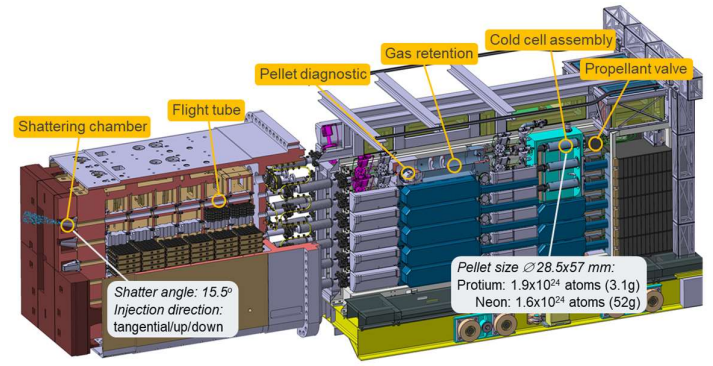


Fig. 1: Shattered pellet injector components in one of the EP cells. This particular port plug hosts twelve injectors.

Following the final design review last year, the DMS is now being brought to the maturity required for manufacturing. As part of the design development, new production techniques, such as electroforming, have been qualified for the cold-cell assembly to improve the thermal coupling and integration of complex heat exchanger geometries and ancillaries. The design is tailored for 28.5 mm diameter and 57 mm long pellets (referred to as "baseline pellet"), but also has the flexibility to adapt to smaller pellet sizes which are required for the Start of Research Operation (SRO) campaign. The pellets are dislodged and accelerated to an envisaged nominal velocity of 500 m/s for H pellets by injecting high pressure gas, using a fast valve operating in the range of 1 ms, into the breech volume between the pellet and the valve orifice. The final pellet velocity is the result of a complex interplay of 1) breakaway pressure, imposed by the shear strength, pellet formation recipe, cold zone temperature and pellet aspect ratio, 2) the breech volume, its shape optimised for the gas flow and its length minimised for good velocity control while providing sufficient thermal separation of the cold cell and warm propellant valve, and 3) the delivered gas amount.

The DMS must be capable of forming pellets using supercritical helium (SHe) within 30 minutes to comply with

the duty cycle of ITER. A pre-prototype cold head including gas pre-cooler and gradient temperature control was designed and tested with SHe at flow rate of 0.3 g/s, similar to what is expected from ITER's cryogenic supply. The so-called "hot pre-injection" pellet formation process has been compared for three different cryogenic coolants, liquid helium (LHe), gaseous helium (GHe) and SHe in the TYFANIES test bench [11]. The cold cell is first filled with gas to a pressure of 72 mbar while kept at temperatures above the triple point of H (13.95 K). Following the cool down (see Fig. 2a) and the initial desublimation, the supplied gas flow is controlled by keeping the pressure in the cold cell constant. The corresponding pellet mass rise is shown in figure 2b. Due to the slower cool down and hence reduced desublimation rate for SHe or GHe, the formation time is 5-6 min longer but still remains within the 30 min target even for cold cell temperatures around 6 K (c.f. Fig. 2c).

The cold cell assembly design incorporates also an axial symmetric gas feed to reduce the buoyancy effect during the formation, which has been numerically studied in [14], leading to slanted fronts and ends of the pellet. The main issue which can arise from this effect is a torque due to the back

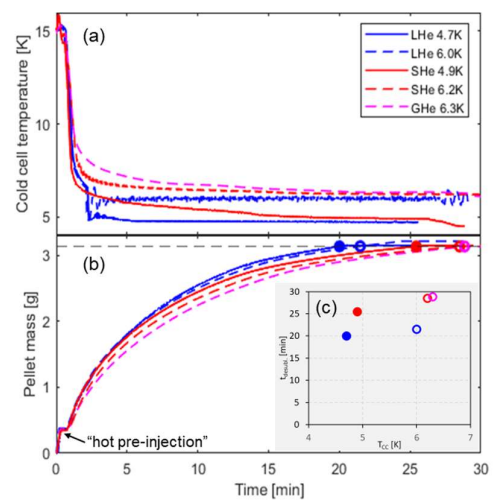
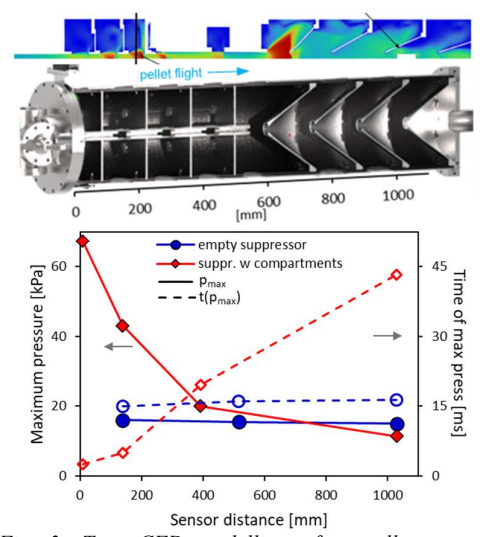


Fig. 2: Time traces of H desublimation process: (a) cold cell temperature, (b) corresponding pellet mass derived from integrated gas flow with the black dashed line indicating the nominal required pellet mass. Insert (c) shows desublimation duration for a baseline DMS pellet as function of cold cell temperature, grouped by different cryogenic coolant supply.

pressure on the pellet when it leaves the acceleration tube causing it to gyrate and potentially collide with gate valve orifices in the flight line. CFD modelling has revealed that the torque becomes negligible if the pressure at the pellet back falls below 10 kPa. To achieve this and to retain the propellant gas, which can deteriorate the mitigation efficiency due to premature cooling of the plasma, a propellant suppressor design was developed using a combination of compartments and funnels to impede the flow of gas and debris. The latter might be produced during the pellet dislodgement and arrive in the plasma ahead of the main fragment cloud causing undesirable cooling of the plasma. The design of the gas suppressor has been guided by CFD modelling of the gas flow including the moving pellet, which will aid the gas blocking. Figure 3 top shows the pressure distribution in the two suppressor stages at a time when the pellet (white rectangle) is about to leave the suppressor. The gas is not only retained in the first three Fig. 3: Top: CFD modelling of propellant gas compartments but also the inverted funnels help to impede the retention for the latest suppressor design, crossgas flow. The length of the openings in the guide tube inside section through suppressor mock-up. Bottom: the suppressor is chosen such that the pellet cannot be overtaken magnitude and time of maximum pressure for by the gas.

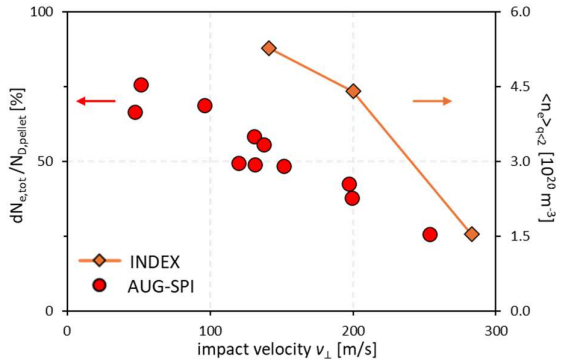


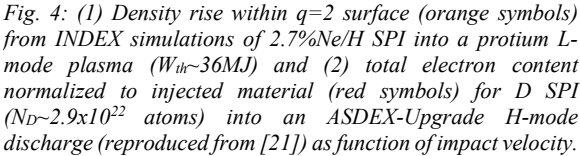
suppressor without and with compartments.

An issue arose from the observation that some material remains in the cold zone or is removed from the pellet during the launch, leaving a gap of about 0.1 mm around the pellet. CFD simulations of the gas propagation inside the suppressor with a similar gap size predicts a factor 100 larger gas outflow at the time the pellet leaves the suppressor than for a full diameter pellet. While this has a significant effect on the performance of the suppressor and the pellet back pressure, the amount of gas arriving at the plasma edge prior the fragment arrival is still expected to be $\sim 10^{23}$ H-atoms per second, which is well below the maximum tolerable amount to avoid premature initiation of the thermal quench (TQ). The pressure evolution inside the suppressor volume has been measured in the DMS Support Laboratory [10]. If no obstructions are used, the pressure rise inside the suppressor is almost simultaneous (bottom plot in Fig. 3) and only ~7.4 barL of propellant gas is retained. Incorporating the first set of compartments, the gas can be effectively blocked as indicated by the large pressure distribution across the suppressor and about 8.8 barL can be retained by the time the pellet reaches the shattering unit. One should note that the pressure in the last part of the suppressor measured at a position close to the exit is just at the pressure limit below which pellet gyration might be avoided. To reduce the possibility of pellet movement orthogonal to its longitudinal flight direction, which might be caused by gas forming due to the Leidenfrost effect and to avoid premature pellet breakage, rails have been introduced to guide the pellet through the obstructions and to minimise the contact area with the pellet. The final confirmation that sufficient gas has been retained is pending ongoing modelling taking into account all non-ideal situations of the pellet launch. As further risk mitigations, a fast vacuum shutter which closes in ~2 ms has been developed [15] and was tested in an ambient magnetic field. In addition, the concept of a mechanical pellet launcher, which uses no propellant gas for the acceleration, is about to be tested.

Maximising the assimilation of the injected material in the plasma is crucial for effective disruption mitigation. The optimum fragment size and velocity distribution were derived through modelling and supported by experiments conducted on several tokamaks within the ITER members' institutes. The injected fragment plume can be characterized by its size and velocity distribution, velocity dispersion and spatial width. All these parameters can be varied to some extent through the shattering geometry, pellet velocity and pellet size. However, large changes in the pellet impact location on the shattering plane will also alter the fragment plume.

The densification of the plasma prior to the current quench (CQ) is key for successful RE avoidance for which the density rise inside the q=2 surface is a figure of merit. The influence of the fragment size and velocity distribution and velocity dispersion on this density has been studied for various ITER target plasmas with the 1.5D INDEX code [16]. An example of the impact of the fragment size distribution (FSD) on the material assimilation in a protium L-mode plasma, plasma current Ip of 15 MA and thermal energy Wth of 36 MJ, as foreseen in SRO (c.f. section 3) is shown in figure 4. The impact velocity $v_{\perp} = v_{\text{pellet}} \sin(\alpha)$, with v_{pellet} as pellet velocity and α as shattering angle, can be used as a proxy for the FSD. A full-size pellet containing 5x10²² Ne and 1.8x10²⁴ H-atoms





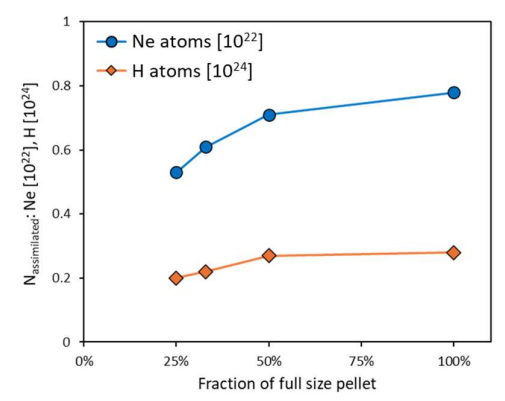


Fig. 5: Assimilated amount of Ne- and H-atoms as function of pellet size normalized to baseline pellet size of \varnothing =28.5 mm x L=57 mm simulated with INDEX. Note the 100 times larger scale for H.

was considered to be fragmented in the simulation according to the statistical fragmentation model by Parks [17]. At that time of these simulations the threshold velocity below which a pellet survives a shallow impact [18] was not known for protium and the value of 20 m/s for deuterium was used instead. The simulations predict a larger density rise and hence better assimilation for lower v_{\perp} , i.e. for larger fragments. The smaller total surface of the fragments gives less ablation in the edge and enables better core deposition of the material. Therefore, the baseline design of the DMS foresees a shattering angle of 15.5° in the equatorial ports and a nominal pellet velocity of 500 m/s, which corresponds to impact velocity on the shatter surface of 133 m/s.

To study the effect of the fragment plume characteristics in more detail, a SPI system comprising different shattering geometries to disentangle the FSD and injection velocity has been installed at ASDEX-Upgrade (AUG) [19,20]. In a series of experiments the impact velocity was varied for SPI of a deuterium (D) pellet into a H-mode plasma ($I_p \sim 0.8$ MA, $q_{95} \sim 3.7$, $P_{aux} \sim 14$ MW) with a W_{th} of ~600 kJ and a pre-SPI electron content of ~6x10²⁰ [21]. The experimental results (red symbols in Fig. 4) confirm the general trend that larger fragments lead to better assimilation. Considering that the ablation rate drastically drops below temperatures of 100eV, the estimated maximum assimilation is $1.3x10^{22}$, or $1.5x10^{22}$ if reheating before the TQ onset is taken into account, the data suggest that only below impact velocities of ~100 m/s a cooling of the entire plasma through D injection is expected. Of course, the optimised fragment size and velocity distribution will depend on the plasma properties at the time of injection and especially in plasmas which are about to disrupt for instance due to impurity accumulation the assimilation will be deteriorated. This is presently subject of new modelling activities of the DMS TF.

Experiments and modelling have indicated that the assimilation is limited depending on the plasma energy.

INDEX modelling suggests that for a 15 MA L-mode plasma only 16% of the baseline pellet is assimilated but that this fraction can reach 44% for quarter-size pellets. Figure 5 illustrates the absolute number of assimilated Ne and H as function of pellet size. It is evident that for pellets larger than half size the additional gain in assimilation is minimal. Therefore, the set of cold cell assemblies of the equatorial port injectors of the ITER DMS will allow the injection of quarter-size, half-size and full-size pellets during SRO. One should nevertheless note that reducing the pellet size will result in smaller fragments and reducing the pellet velocity with the same type of propellant valve is difficult. The cartridge design of the cold cell assembly allows a fast change of the pellet sizes after SRO in preparation for the fusion power operation (FPO).

The question of how to achieve the optimum fragment plume characteristics was addressed in two ways: a dedicated test bench was built to characterize the fragment plume for different

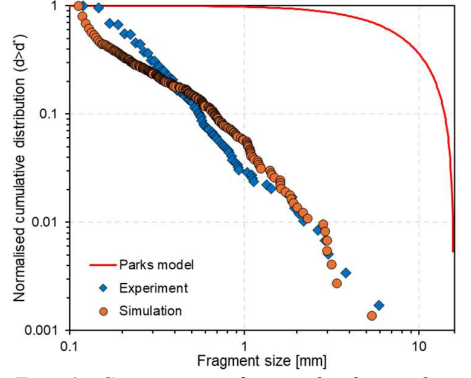


Fig. 6: Comparison of normalized cumulative fragment size distributions versus fragment size from shattering experiment, simulation and statistical fragmentation model. The data refer to D pellet (\varnothing =28.5 mm x L=57 mm) with an impact velocity \sim 38 m/s.

shattering geometries [10], and a code based on a discrete element method was developed to simulate the fragmentation [22, 23]. In a first step, material parameters, such as bulk modulus and fracture strength of D and Ne, were calibrated and validated using fast camera recordings of laboratory shattering tests of the AUG-SPI. Due to the unavailability of shattering videos of H pellets, the material properties were extrapolated using the solid-state density of protium. Figure 6 shows an example of the experimentally measured FSD determined through a tracking algorithm and the simulation results using the previously determined material parameters and the actual

shattering geometry. The agreement with the experiment is remarkable and the capabilities of the code has been demonstrated across several shattering tests with different velocities and material. As further comparison, the FSD determined by Parks's model is shown. This model tends to overpredict large fragments and ignores any changes to the FSD due to specifics of the shattering geometry such as length of shatter plane and cross-section. Simulations have shown that the fragments experience additional break-up before leaving the shatter head. A comparison of AUG-SPI shattering characterisation with Parks's model showed a dependence of the parameter C, empirically determined in [18], with the fragmentation parameter $X_R = (v_{\perp}/v_{\text{thres}})^2$. The agreement with the statistical fragmentation model can be improved by applying a fit that reveals for deuterium $C \sim X_R^{-1.13}$ based on available data [24]. The parameters C and v_{thresh} likely depend also on the exact shattering geometry and pellet size.

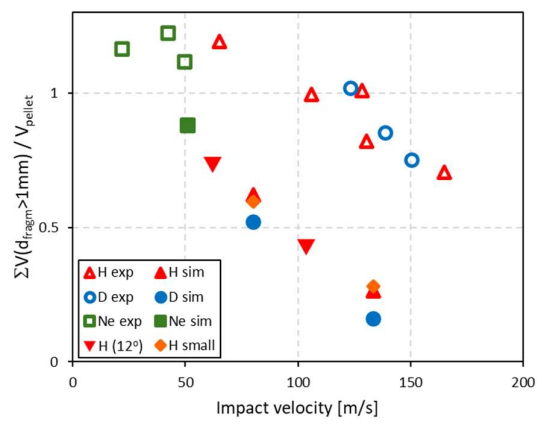


Fig. 7: Cumulative fragment volume (normalized to the original pellet volume) as function of impact velocity as measured with laser curtain diagnostic and as predicted by simulations. The "small" H pellet corresponds to a third of the baseline pellet.

Characterising the fragment plume of shattered ITER DMS baseline pellets is a challenge due to the huge amount of material and fragments, which will partially mask each other. Therefore, the diagnostic chamber of the DMS Support Laboratory was equipped with laser curtains intersecting the fragments. The results are summarized in figure 7 showing the accumulated volume for fragments > 1 mm. The experimental data are an average of a few samples with similar impact velocity (open symbols). In the experiments no clear difference between H (red) and D (blue) pellets could be seen in the FSDs, contrary to what would be expected from a higher threshold velocity of H of 26 m/s. In general, the number of large fragments decreases with increasing impact velocity. However, from the data at low v_{\perp} it is evident that the volumes of large fragments might be overestimated. To gain more insight into the uncertainty of the measurements, synthetic laser curtain data have been produced from the full 3D output of the simulations. The simulations (full symbols) qualitatively reproduce the trend. For deuterium the FSD is expected to shift towards small fragments as suggest by the lower threshold velocity. This has also been observed in the simulations (blue data points).

The shattering chamber must survive over the entire ITER operational life several thousands of pellet impacts with kinetic energies up to 1.6 kJ. The resulting plastic strain has been modelled with LS-DYNA after determining the force time response of H and Ne with a perpendicular impact on a Hopkinson-bar in a test bench [11]. The analysis revealed that the shatter chamber could withstand only a few Ne pellet impacts. The neutron loading and limited cooling made it impossible to further strengthen the component. Therefore, it was decided to make the shattering section part of the stainless-steel diagnostic first wall (DFW). The UP injectors are dedicated to post-TQ injection and a steep shattering angle of 35° was planned to produce mainly micro-fragments and gas. However, this turned out to be incompatible with integration into the port plug and DFW. Given the geometrical constraints, the shattering section will consist of two shatter planes turned into the toroidal direction to ensure a good intersection of the injected material with the plasma. The brown area in figure 8 indicates the plume projected back onto a poloidal plane. The majority of the fragments are expected to be on the high field side. The equilibrium shown corresponds to a major disruption at 50 ms after a vertical displacement of -20 cm would have been detected.

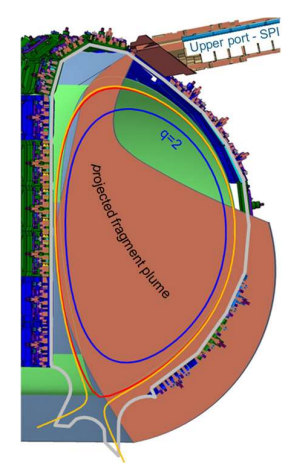


Fig. 8: UP injection geometry with equilibrium of a vertical unstable major disruption.

3. STRATEGY FOR APPLICATION OF THE DMS DURING ITER OPERATION

A significant part of the first ITER campaign in the 2024 re-baseline (SRO) [25], is devoted to the optimisation of the DMS for effective disruption mitigation. The change of the first wall material from beryllium (Be) to tungsten (W) in the new baseline has relaxed some of the mitigation requirements [26] as shown in figure 9,

allowing exploration of the different DMS injection schemes to be tested at lower plasma currents without fear of damaging the W armour. Mitigation of thermal loads resulting from deposited magnetic energy will become mandatory for $I_p > 11$ MA, which is already planned in SRO with hydrogen plasmas in preparation for the FPO campaigns. The electromagnetic load (EML) limits remain unchanged and CQ control might be required already for I_p above 8.4 MA depending on the results from the disruption load characterisation. The raised thermal load limits give the possibility to reduce the amount of injected Ne aiming at slower CQs while remaining within the limit imposed by halo currents. This will help to reduce the risk of RE generation during the CQ. In parallel with the stepwise increase of I_p and W_{th} during the different SRO phases, the possible disruption loads will be assessed through deliberate disruptions and the mitigation targets and disruption budget consumption constantly revised. The

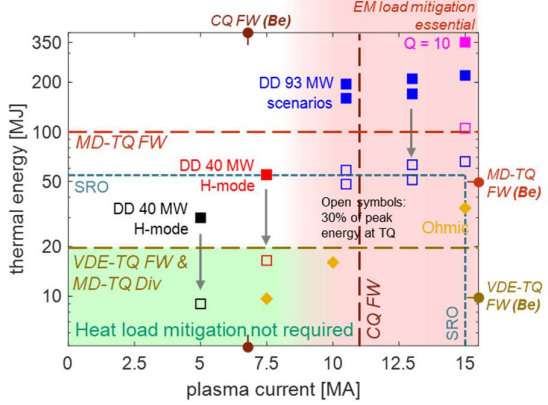


Fig. 9: Thermal load (TL) and electromagnetic load (EML) limits (dashed lines) for W first wall (FW) and divertor. Symbols refer to the pre-disruption W_{th} and Ip for scenarios planned during SRO and FPO. The green area corresponds to the space where no thermal load mitigation is required, whereas the red area indicates the range of Ip for which EML mitigation is needed.

impact of RE is of large concern and the inertially cooled W FW during SRO allows a safe examination of possible mitigation schemes. These tests will commence already during limiter operation and will continue up to the maximum safe I_p (possibly 7.5 MA) before the start of DD plasmas. Depending on the viability of the RE impact mitigation scheme, the tests will continue up to 15 MA in the last phases of SRO. Although the plasma thermal energies in SRO are not expected to exceed 60MJ, the electron temperature in EC-heated plasmas might reach 10-20 keV, allowing the examination of RE avoidance for hot tail RE seeds in addition to assessing the secondary seed resulting from the avalanche gain for I_p up to 15MA. At the conclusion of SRO, the mitigation of TLs and EMLs is expected to be demonstrated for $W_{th} \sim 60$ MJ, $W_{mag} \sim 400$ MJ and I_p up to 15 MA, and the suppression of hot-tail RE seeds to be achieved. The first campaign during FPO will have a phase with protium+tritium plasmas, which will give the possibility to study RE avoidance for β -decay electron seeds. Since plasma scenarios with constantly increasing thermal energies will be developed during FPO, the DMS injection schemes will be continuously optimised.

Various injection schemes are envisaged to fulfil the mitigation targets. These schemes can be categorised by the disruption phase when they are executed: 1) multiple mixed-pellet SPI or staggered SPI injections before MHD leads to a global reconnection event (GRE) and the TQ, 2) mixed-pellet SPI after the GRE (or post-TQ) to at least mitigate thermal loads of the magnetic energy, control of CQ duration and to densify the plasma for RE avoidance, and 3) post-TQ low-Z (H) or high-Z (Ne) SPI for RE impact mitigation. The viability of these injection schemes will be assessed based on the material assimilation for densification, robustness of CQ control and the implication for the overall reliability of the DMS demanding different combinations of pellet injections. The required amounts of Ne and H assimilated in the plasma to fulfil the DMS mitigation functions are summarized in Table 1 [12]. The EML mitigation sets the lower boundary for the required Ne quantity. As can be inferred from the table, a

| Purpose | Injection time | Required amount [atoms] | | |
|-----------------------------------|-------------------|---|--|--|
| TL mitigation (Wth) | pre-TQ | $> 1x10^{21}$ Ne (mixed with H) | | |
| TL mitigation (W _{mag}) | pre-TQ or post-TQ | $> 2x10^{21}$ Ne | | |
| EML mitigation (CQ control) | pre-TQ or post-TQ | $> 5 \times 10^{21}$ Ne and $< 3.5 \times 10^{22}$ Ne | | |
| RE avoidance | pre-TQ | SRO: ~2x10 ²³ H | | |
| RE avoidance | pre-1Q | FPO (DT): ~2x10 ²⁴ H | | |
| DE impact low-Z | post-TQ | ~1-8x10 ²³ H | | |
| RE impact high-Z | post-TQ | ~1x10 ²⁵ Ne | | |

Table 1: Required amount of assimilated Ne and H for the different the mitigation functions.

significant amount protium is required to achieve the desired density for RE avoidance. In particular in degraded plasmas, where for instance core cooling occurred already due to impurity accumulation, this poses a challenge because of the low material assimilation. One notes that the high-Z RE impact mitigation scheme is also demanding because a baseline pellet contains only $\sim 1.6 \times 10^{24}$ Ne atoms.

A possible configuration of the DMS using different injection schemes for a 15 MA DT H-mode plasma with expected $W_{th} \sim 350$ MJ is shown in Table 2. Depending on the plasma phase, either mixed Ne/H or staggered injection will be used provided the TQ did not yet occur. The assimilation fractions have been taken from INDEX modelling except for the RE impact mitigation. Prior to the change of the wall material from Be to W, the radiation flash during the TL mitigation required for mixed Ne/H the simultaneous injection from different toroidal locations which has been modelled with JOREK [27]. This requirement could now be relaxed, and the potential jitter of the injections is less problematic. Notable is that the poor assimilation in the L-mode phase requires a substantial number of pellets for RE avoidance. Overall, the DMS capability still provides sufficient redundancy for the EP-SPI, eleven pellets in case of RE impact mitigation with low-Z and six pellets for RE mitigation with high-Z.

| Scheme | | Plasma | Injection | Pellets | Inject. Amount | Assimil. | Assimil. amount |
|-------------|----------|--------|-----------|---------|-----------------------------|----------|--------------------------|
| | | phase | time | [#] | [10 ²⁴ atoms] | fraction | [10 ²⁴ atoms] |
| Mixed Ne/I | H | low Ip | pre-TQ | 1 | 0.033 Ne+1.83 H | 15% | 0.005 Ne+0.27 H |
| Staggered I | H + Ne/H | L-mode | pre-TQ | 7 & 1 | 13.3 H & 0.033 Ne+1.83 H | 15% | 0.005 Ne+2.3 H |
| Mixed Ne/H | H | H-mode | pre-TQ | 2 | 0.0064 Ne+3.7 H | 78% | 0.005 Ne+2.9 H |
| post-TQ | | N/A | post-TQ | 1 | 0.033 Ne+1.83 H | 15% | 0.005 Ne+0.27 H |
| RE impact | low-Z | N/A | post-TQ | 2 | 3.8 H | 30% | 1.1 H |
| | high-Z | N/A | post-TQ | 7 | 11 Ne | 100% | 11 Ne |

Table 2: Possible DMS configuration for a 15MA DT H-mode plasma assuming assimilation fractions as predicted by INDEX modelling except for RE impact injections for which the numbers are only indicative.

The staggered injection scheme has several advantages compared to the mixed Ne/H SPI: the initial dilution cooling leads to a reduction of the electron temperature, hence lowering the risk of hot-tail RE seeds, and the concurrent lower thermal plasma energy at the time of the TQ onset requires less Ne for TL mitigation. This scheme starts with single or multiple pure H SPI, followed by a Ne/H injection and has been tested in several tokamaks [3, 5]. However, the scheme can be compromised by several effects. First, the plasmoid drift and resulting rocket effect because of the low field side injection limit the fragment penetration and impede core deposition of the material. The possibility of using Ne-doping of the H-pellets to reduce the plasmoid cloud pressure has been studied experimentally and modelled for JET SPI [28]. Though a benefit of trace Ne injection seems to exist, the pre-TQ duration is drastically shortened as can be seen in figure 10a [29]. Even a small amount of Ne reduces the pre-TQ to only for 5 ms making injection of several trace Ne/H pellets impossible.

Second, the large variation of the pre-TQ duration after a pure D injection raises raises concerns for the staggered injection scheme. As shown in figure 10b [29], the pre-TQ duration is governed by the plasma radiation just before the injection. This parameter will be taken into account in the future DMS triggering scheme to determine whether a staggered injection is still feasible. In particular, impurity seeded scenarios as foreseen for ITER to reduce the steady-state power loads on the divertor, might invalidate the application of the staggered injection scheme.

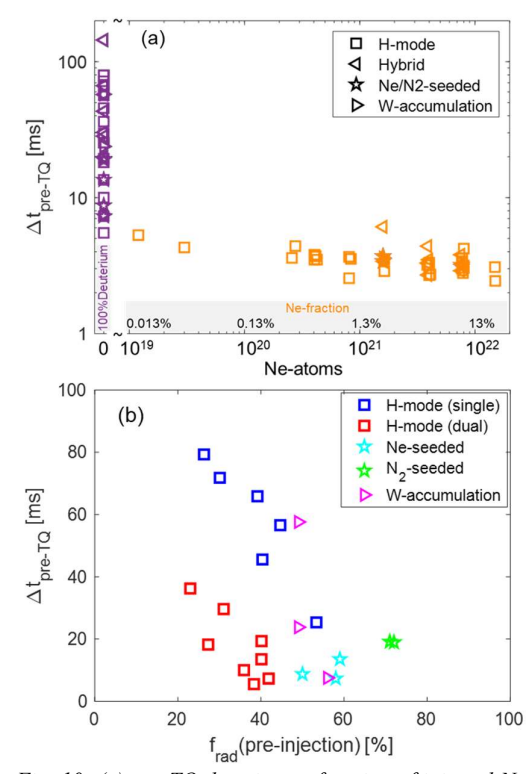


Fig. 10: (a) pre-TQ duration as function of injected Ne into JET plasmas. Symbols indicate different target plasmas. Note the large scatter for pure-D injections (purple data points). (b) pre-TQ duration shown as dependence of pre-injected radiated power fraction for pure-D injections. Reproduced from [29].

Third, the assimilation in degraded plasmas is low and only a fraction of the injected material will be ionised. The majority of the initially injected H will lead to a strong rise of the neutral pressure in the vessel. As a result, in case a RE beam forms, the density of free electrons increases due to ionization caused by RE collisions and the termination of the RE beam becomes less benign. A multi machine comparison has been carried out to predict the upper pressure limit for ITER [30]. Depending on the RE current density, this upper pressure limit is predicted to be 1.5-3 Pa which limits the injection to 0.9-1.7x10²⁴ H-atoms. Therefore, smaller pellets might be essential to obtain benign RE terminations. Moreover, this upper pressure limit is in conflict with the requirements for RE avoidance especially in case of low material assimilation. These findings led to a revision of the cold cell configuration of the DMS in SRO to accommodate a range of different pellet sizes. The final configuration for FPO will be then refined based on the outcome of the disruption mitigation experiments during SRO.

4. SUMMARY AND OUTLOOK

The disruption mitigation system at ITER is highly flexible to optimise the injection of Ne and H in case a disruption is detected. The integration of SPIs into the challenging environment of ITER, such as neutron loading, space restriction, ambient magnetic fields and limited access, required the establishment of new design solutions. The R&D programme launched by the ITER Organization to develop the physics basis and technology will continue to further consolidate the design and to prepare for the future operation of the DMS. Test benches with ITER-size pellets for SPI are now operated routinely in three laboratories. The formation and launch of pellets are well understood. Various techniques are considered for optimum trajectory control of the pellet travel.

The viability of disruption mitigation schemes with SPI is being extensively assessed experimentally and through modelling. A few issues still need to be addressed, for example such as the optimum pellet size for low energy plasmas and plasma with pre-existing instabilities, feasibility of plasmoid suppression using Ne doped H pellets, access to RE benign termination in ITER. In addition to the inclusion of an inertially cooled provisional first wall for the SRO phase of the new baseline, allowing safer testing of the DMS before DT operations, the outcome of all ongoing activities will further consolidate predictions for ITER and reduce the time needed for optimizing the DMS injection schemes.

DISCLAIMER

The ITER is the Nuclear Facility INB No. 174. The views and opinions expressed herein do not necessarily reflect those of the ITER Organization. This work has been carried out within the framework of the EUROfusion Consortium and has received funding from the Euratom research and training programme 2014-2018 under grant agreement No 633053. The Swiss contribution to this work has been funded by the Swiss State Secretariat for Education, Research and Innovation (SERI). This work was supported in part by the Swiss National Science Foundation. Views and opinions expressed are however those of the author(s) only and do not necessarily reflect those of the European Union, the European Commission or SERI.

REFERENCES

- [1] COMMAUX, N., et al., Nucl.Fus. 56 (2016), 046007
- [2] KIM J. H., et al., Proc. 28th IAEA FEC (2020).
- [3] SHIRAKI, D., et al., Proc. 28th IAEA FEC (2020).
- [4] LI, Y., et al., Nucl. Fus. 61 (2021) 126025.
- [5] JACHMICH, S., et al., Nucl. Fusion 62 (2022) 026012.
- [6] YUAN, J.S., et al., Nucl. Fus. 63 (2023) 106008.
- [7] SHEIKH, U., et al., Nucl. Fus. 65 (2025) 036035.
- [8] VINYAR, I., et al., Instruments and Experimental Techniques 49, #5 (2006) 717.
- [9] GEBHART, T., et al., Nucl. Fus. 61 (2021), 106007.
- [10] ZOLETNIK, S., et al., Fus. Eng. Des. 190 (2023), 113701.
- [11] MANZAGOL, J., et al., IEEE Trans. Plasm. Sci. 52 (2024), 3936.
- [12] LEHNEN, M., et al., 29th IAEA Fusion Energy Conference 2023, London, U.K.
- [13] LEHNEN, M., et al., 27th IAEA Fusion Energy Conference 2018, Ahmedabad, India, EX/P7-12.
- [14] ADONG, F., et al., Int. Journal Heat & Mass Transfer 252 (2025), 127087.
- [15] REFY, D.I., et al., Fus. Eng. Des. 216 (2025), 115089.
- [16] MATSUYAMA, A., et al., Plasm. Phys. Contr. Fus. 64 (2022), 105018.
- [17] PARKS, P., "Modelling dynamic fracture of cryogenic pellets," Tech. Rep. GA-A28325, USA (2016).
- [18] GEBHART, T., et al., IEEE Trans. Plas. Sci. 48 (2020), 2957968.
- [19] DIBON, M., et al., Rev.Sci.Ins. 95 (2023), 043504.
- [20] HEINRICH, P., et al., Fus. Eng. Des. 206 (2024), 114576.
- [21] JACHMICH, S., et al., Proc. 49th EPS Conference, Bordeaux, France (2023), O2.103.
- [22] SIGNETTI, S., et al., Proceedings of the 17th Hypervelocity Impact Symposium, Tsukuba, Japan (2024).
- [23] MATURA, P., et al., Proceedings of the 17th Hypervelocity Impact Symposium, Tsukuba, Japan (2024).
- [24] MATURA, P., et al., 3rd IAEA Technical Meeting on Plasma Disruptions and their Mitigation, 2024.
- [25] LOARTE, A., et al., Plasm.Phys.Contr.Fus 67 (2025), 065023.
- [26] ARTOLA, F.J., et al., this conference, paper IAEA-CN-316-2762.
- [27] HU, D., et al., this conference, paper IAEA-CN-316-2678.
- [28] KONG, M., et al., this conference, paper IAEA-CN-316-2799.
- [29] JACHMICH, S., et al., 50th EPS Conference, Salamanca, Spain (2024), I.303, to be published.
- [30] SHEIKH, U., et al., this conference, paper IAEA-CN-316-2818.